Braz J Phys (2014) 44:19–29
DOI 10.1007/s13538-013-0174-6

SOCIEDADE BRASILEIRA DE FÍSICA

ATOMIC PHYSICS

Geometry in the Entanglement Dynamics of the Double Jaynes–Cummings Model

A. R. Vieira · J. G. G. de Oliveira Junior · J. G. Peixoto de Faria · M. C. Nemes

Received: 24 October 2012 / Published online: 20 December 2013

Abstract We report on the geometric character of the entanglement dynamics of two pairs of *qubits* evolving according to the double Jaynes–Cummings model. We show that the entanglement dynamics for the initial states $|\psi_0\rangle = \cos\alpha|10\rangle + \sin\alpha|01\rangle$ and $|\phi_0\rangle = \cos\alpha|11\rangle + \sin\alpha|00\rangle$ cover three-dimensional surfaces in the diagram $C_{ij} \times C_{ik} \times C_{il}$, where C_{mn} stands for the concurrence between qubits m and n, varying $0 \leq \alpha \leq \pi/2$. In the first case, projections of the surfaces on a diagram $C_{ij} \times C_{kl}$ are conics. In the second case, curves can be more complex. We relate those conics with a measurable quantity, the *predictability*. We also derive inequalities limiting the sum of the squares of the concurrence of every bipartition and show that sudden death of entanglement is intimately connected to the size of the average radius of a hypersphere.

Keywords Entanglement · Geometry · Jaynes–Cummings model · Predictability

A. R. Vieira (✉) · M. C. Nemes
Departamento de Física, CP 702, Universidade Federal de Minas Gerais, 30123-970, Belo Horizonte, MG, Brazil
e-mail: arvieira@fisica.ufmg.br

M. C. Nemes
e-mail: carolina@fisica.ufmg.br

J. G. G. de Oliveira Junior
Centro de Formação de Professores, Universidade Federal do Recôncavo da Bahia, 45.300-000, Amargosa, BA, Brazil
e-mail: zgeraldo@ufrb.edu.br

J. G. Peixoto de Faria
Departamento Acadêmico de Disciplinas Básicas, Centro Federal de Educação Tecnológica de Minas Gerais, 30510-000, Belo Horizonte, MG, Brazil
e-mail: jgpfaria@des.cefetmg.br

1 Introduction

The capacity of quantum systems to entangle is perhaps the most intriguing aspect of quantum mechanics and is a feature that distinguishes classical from quantum physics. In a seminal work, Einstein et al. [1] have brought this property to discussion and the subject has been investigated since then. Recently, pure bipartite interacting quantum systems have proven to be a very useful tool to explore entanglement dynamics and unveil several of the intriguing properties which govern quantum correlations exchange. Examples of such properties are the sudden (or asymptotic) disappearance of entanglement [2–5], the so called entanglement sudden birth [6], control of entanglement dynamics [7], and entanglement distribution [8], an important ingredient for quantum computation. Perhaps the best known and explored model is the Jaynes–Cummings Model (JCM) [9], where several dynamical scenarios have been explored both with and without dissipation. An analogous model, the Tavis–Cummings model [10] has also been used for similar purposes. The result obtained in these two contexts have enlightened entanglement disappearance in finite time [11–13], relations between purity, energy, and entanglement [14, 15], invariant entanglement [16], and general aspects of entanglement dynamics between partitions [17–20]. In the present work, we show that the entanglement dynamics of the Double Jaynes–Cummings Model (DJCM) [11] exhibits geometric properties for the two classes of initial states we considered. The scenario is a pair of initially entangled non-interacting atoms "A" and "B", two cavities "a" and "b", which interact locally via the JCM, and we use concurrence [21] to quantify entanglement between these parts. We show that, for initial atomic states belonging to the class $|\psi_0\rangle = \cos\alpha|10\rangle + \sin\alpha|01\rangle$, the relations between concurrences describe a conic in a diagram $C_{ij} \times C_{kl}$, with $ij \neq kl$

(*ij* being equal to *Aa*, *Ab*, *AB*, *ab*, *aB*, and *Bb*). On the other hand, if the initial atomic state belongs to the class $|\phi_0\rangle = \cos\alpha|11\rangle + \sin\alpha|00\rangle$, the geometric curve is not as simple. However, in all cases when a conic is found, the eccentricity can be written as a function of the absolute value of the average excitations in *A*, in other words: $\mathcal{P}_0 = \left|\mathrm{tr}\left(\sigma_z^A \rho_0\right)\right|$. If the initial atomic state is $|\psi_0\rangle$, $\mathcal{P}_0$ gives the probability of the excitation being found in only one of the two bipartition *Aa* or *Bb*. On the other hand, if the initial state is $|\phi_0\rangle$, $\mathcal{P}_0$ does not have the same interpretation. It is important to notice that $\mathcal{P}_0$ is the *predictability*, which according to the complementarity relation between two *qubits* proposed in ref. [22], is related to the initial concurrence. We find that this geometric character can be extended for more dimensions. It is possible to define a hypersurface over which the concurrence dynamics between every two pairs *i* and *j* defines a trajectory over or inside this hyper surface.

The present work is organized as follows: In Section 2, we present the physical model and the time evolution for the two classes of states, $|\psi_0\rangle$ and $|\phi_0\rangle$; next, in Section 3, we determine the entanglement (quantified by concurrence), and we construct the diagram $C_{ij} \times C_{kl}$ showing that whenever a conic is found, its eccentricity is related to the predictability as defined in [22]; in the following section, we show the existence of an entanglement surface for the dynamics of the pairs of concurrences involving the same qubit and justify why curves of the diagrams $C_{ij} \times C_{kl}$ will be over that surface; In Section 5, we find an inequality which describes the entanglement dynamics of all qubit pairs; In Section 6, we present how decoherence affects some of the conics, and we conclude in Section 7.

2 The Physical Model

Consider a composite system of two identical two-level atoms ("*A*" and "*B*") and two identical cavities ("*a*" and "*b*"). The atom "*A*" ("*B*") interacts resonantly with the cavity "*a*" ("*b*"), respectively, via JCM [9] and the evolution of the system is governed by the Hamiltonian

$$H = \hbar\omega a^\dagger a + \hbar\omega b^\dagger b + \frac{\hbar\omega}{2}\sigma_z^A + \frac{\hbar\omega}{2}\sigma_z^B + g\left(a^\dagger\sigma_-^A + a\sigma_+^A\right) + g\left(b^\dagger\sigma_-^B + b\sigma_+^B\right), \quad (1)$$

where $a^\dagger$ ($b^\dagger$) and a (b) are the *creation* and *annihilation* operators of the field inside cavity a (b), respectively. The matrices σ_-^i, σ_+^i, and σ_z^i are Pauli matrices of the ith atom, with $i = A, B$. The cavities are resonant with the atoms, i.e., the frequency of the field inside each cavity is equal to the frequency of the atomic transition of the atoms' internal levels (Fig. 1) .

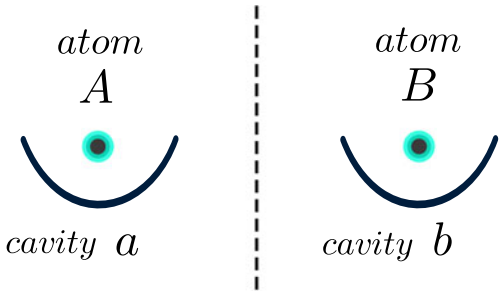

Fig. 1 A schematic figure of the DJCM. In the *left* (*right*) partition there is the atom "*A*" ("*B*") interacting with the cavity "*a*" ("*b*"), respectively, and there is no interaction between the partition "*Aa*" and "*Bb*"

We consider the cavities initially in the vacuum state and some entanglement between the atoms. Consider the initial state of the system as

$$|\psi_0\rangle = (\cos\alpha|10\rangle + \sin\alpha|01\rangle) \otimes |00\rangle. \quad (2)$$

Because of the conservation of the number of excitations, the time evolution can be determined analytically and it reads

$$|\psi_t\rangle = x_1(t)|10\rangle|00\rangle + x_2(t)|01\rangle|00\rangle + x_3(t)|00\rangle|10\rangle + x_4(t)|00\rangle|01\rangle. \quad (3)$$

The coefficients will be given by the Schrödinger equation, $i|\dot{\psi}_t\rangle = H|\psi_t\rangle$, plus the boundary conditions $x_1(0) = \cos\alpha$, $x_2(0) = \sin\alpha$, $x_3(0) = 0$ and $x_4(0) = 0$. They are

$$x_1(t) = \cos\alpha\cos(gt), \quad (4)$$
$$x_2(t) = \sin\alpha\cos(gt), \quad (5)$$
$$x_3(t) = -i\cos\alpha\sin(gt), \quad (6)$$
$$x_4(t) = -i\sin\alpha\sin(gt). \quad (7)$$

Consider also the initial state

$$|\phi_0\rangle = (\cos\alpha|11\rangle + \sin\alpha|00\rangle) \otimes |00\rangle. \quad (8)$$

The same thing can be done to find the time evolution. We have

$$|\phi_t\rangle = y_1(t)|11\rangle|00\rangle + y_2(t)|00\rangle|00\rangle + y_3(t)|10\rangle|01\rangle + y_4(t)|01\rangle|10\rangle + y_5(t)|00\rangle|11\rangle, \quad (9)$$

where

$$y_1(t) = e^{-i\omega t}\cos\alpha\cos^2(gt), \quad (10)$$
$$y_2(t) = e^{i\omega t}\sin\alpha, \quad (11)$$
$$y_3(t) = -i\,e^{-i\omega t}\cos\alpha\sin(gt)\cos(gt), \quad (12)$$
$$y_4(t) = -i\,e^{-i\omega t}\cos\alpha\sin(gt)\cos(gt), \quad (13)$$
$$y_5(t) = -e^{-i\omega t}\cos\alpha\sin^2(gt). \quad (14)$$

We can observe that, at time t immediately after $t = 0$, the state (3) and (9) will develop entanglement among all the partitions. However, we will consider the entanglement between qubits (*A*, *B*, *a* e *b*) and their relations. Thus, we

will use as entanglement quantifier the concurrence [21], which is defined as

$$C = \max\left[0, \sqrt{\lambda_1} - \sqrt{\lambda_2} - \sqrt{\lambda_3} - \sqrt{\lambda_4}\right], \tag{15}$$

where λ_i are the eigenvalues, organized in a descending order, of the matrix $\rho(\sigma_y \otimes \sigma_y)\rho^*(\sigma_y \otimes \sigma_y)$.

3 Entanglement Dynamics in the Diagram $C_{ij} \times C_{kl}$

We can easily find the state ρ_{ij} of two qubits taking a partial trace over the remaining subsystem. We next determine all C_{ij}.

3.1 For the Initial State $|\psi_0\rangle$

In this case, we obtain

$$C_{AB} = |\sin 2\alpha| \cos^2(gt), \tag{16}$$
$$C_{ab} = |\sin 2\alpha| \sin^2(gt), \tag{17}$$
$$C_{Aa} = \cos^2\alpha |\sin(2gt)|, \tag{18}$$
$$C_{Ab} = |\sin 2\alpha \sin(gt)\cos(gt)|, \tag{19}$$
$$C_{aB} = |\sin 2\alpha \sin(gt)\cos(gt)|, \tag{20}$$
$$C_{Bb} = \sin^2\alpha |\sin(2gt)|. \tag{21}$$

We analyze the geometric structure of entanglement dynamics in a diagram $C_{ij} \times C_{kl}$. In order to do this, observe that we can sum Eq. (16) with Eq. (17) and we have

$$C_{AB} + C_{ab} = C_0, \tag{22}$$

where $C_0 = |\sin 2\alpha|$ is the initial concurrence between the atoms A and B. We notice that this equation defines a straight line in a diagram $C_{AB} \times C_{ab}$ (see Fig. 2). The lines in Eq. (22), when $\alpha \in (0, \pi/2)$, fill the triangle formed by the axes C_{AB}, C_{ab}, and $C_{AB} + C_{ab} = 1$. In addition, we notice that Eqs. (19) and (20) satisfy

$$C_{Ab} = C_{aB}. \tag{23}$$

This shows a symmetry between the cavity of one of the systems and the atom of the other. We proceed dividing (18) by (21) and we easily find (Fig. 3)

$$C_{Aa} = \frac{\cos^2\alpha}{\sin^2\alpha} C_{Bb}, \tag{24}$$

which is a straight line in the diagram $C_{Aa} \times C_{Bb}$. In the interval $0 < \alpha < \pi/2$, the lines (24) are limited in the region between the lines $C_{Aa} = 0$, $C_{Bb} = 0$ and $C_{Aa} + C_{Bb} = 1$. Equations (22–24) define a straight line in their respective diagram $C_{ij} \times C_{kl}$. The line $C_{Aa} + C_{Bb} = 1$, which represents a conservation of entanglement, is a superior limit in all cases. Using the same procedure, and some simplifications, we find other conics (ellipses, circumferences, and straight lines) which we organize as follows:

3.1.1 Concurrence Between Atoms (or Cavities) Versus Concurrence Between One of the Atoms and Its Cavity

a) $C_{AB(ab)} \times C_{Bb}$:

$$\frac{\left(C_{AB(ab)} - C_0/2\right)^2}{C_0^2/4} + \frac{C_{Bb}^2}{\sin^4\alpha} = 1 \tag{25}$$

b) $C_{AB(ab)} \times C_{Aa}$:

$$\frac{\left(C_{AB(ab)} - C_0/2\right)^2}{C_0^2/4} + \frac{C_{Aa}^2}{\cos^4\alpha} = 1 \tag{26}$$

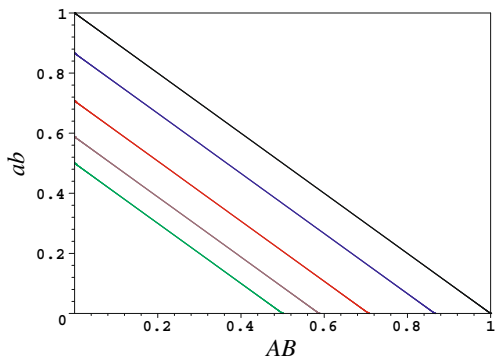

Fig. 2 Graphic of the straight lines $C_{AB} \times C_{ab}$ with $\alpha = \pi/4, \pi/6, \pi/8, \pi/10,$ and $\pi/12$ for the colors *black*, *blue*, *red*, *brown*, and *green*, respectively

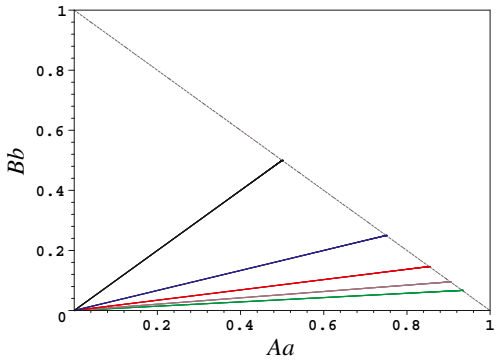

Fig. 3 Graphic of the straight line $C_{Aa} \times C_{Bb}$ with $\alpha = \pi/4, \pi/6, \pi/8, \pi/10,$ and $\pi/12$ for the colors *black*, *blue*, *red*, *brown*, and *green*, respectively. The *slim violet curve* is the straight line $C_{Aa} + C_{Bb} = 1$

3.1.2 Concurrence Between Atoms (or Cavities) Versus Concurrence Between One of the Atoms and the Cavity Which Does Not Contain It

$$\left(C_{AB(ab)} - C_0/2\right)^2 + \left(C_{aB(Ab)}\right)^2 = C_0^2/4 \tag{27}$$

3.1.3 Concurrence Between One of the Atoms and the Cavity Which Does Not Contain It Versus Concurrence Between One of the Atoms And Its Cavity

a) $C_{aB(Ab)} \times C_{Aa}$:

$$C_{aB(Ab)} = \frac{|\sin 2\alpha|}{2\cos^2\alpha} C_{Aa} \tag{28}$$

b) $C_{Ab(aB)} \times C_{Bb}$:

$$C_{Ab(aB)} = \frac{|\sin 2\alpha|}{2\sin^2\alpha} C_{Bb} \tag{29}$$

In order to interpret the expressions (25–29) and their respective figures (Figs. 4, 5, 6, 7, and 8), it becomes instructive to use the predictability,

$$\mathcal{P}_0 = \left|\mathrm{tr}\left(\sigma_z^A \rho_0\right)\right|. \tag{30}$$

We use predictability because, unlike concurrence, it is measurable (the module of the mean value of an observable), local, and it is related to the concurrence [22]. For $\rho_0 = |\psi_0\rangle\langle\psi_0|$, we have $\mathcal{P}_0 = |\cos(2\alpha)|$, and it is clear that $C_0^2 + \mathcal{P}_0^2 = 1$. Observe that when $\mathcal{P}_0 = 0$, the excitation will be equally distributed between the partitions *Aa* and *Bb*, it will not be localized, and the initial entanglement will be maximum between *A* and *B*. On the other hand, if $\mathcal{P}_0 = 1$, the atoms will not be initially entangled and the information if the excitation will be in partition *Aa* or *Bb* will not be available. However, we can assure that the excitation will be in the partition *Aa* or in the partition *Bb*. When $0 < \mathcal{P}_0 < 1$, all we know is that the excitation has a larger probability to be in one of the partitions.

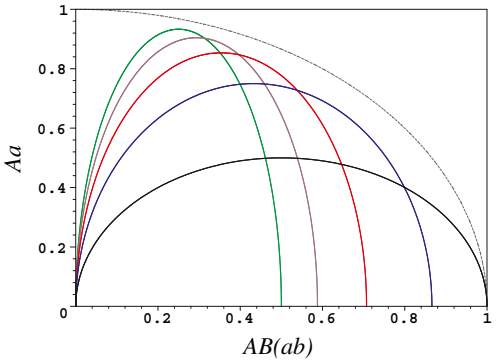

Fig. 5 Graphic of the semiellipse $C_{AB(ab)} \times C_{Aa}$ with $\alpha = \pi/4, \pi/6, \pi/8, \pi/10,$ and $\pi/12$ for the colors *black*, *blue*, *red*, *brown*, and *green*, respectively. The *slim violet curve* is the semicircumference $C_{AB(ab)}^2 + C_{Aa}^2 = 1$

The eccentricity of the ellipses (25) and (26) can be written as a function of the predictability:

$$\epsilon = \sqrt{\frac{2\mathcal{P}_0}{1+\mathcal{P}_0}}. \tag{31}$$

We can determine also the distance f of the focus to the center of each ellipse. For the ellipse (25), the distance of the focus $f^{(a)}$ to its center will be

$$f_{\lessgtr}^{(a)} = \sqrt{\frac{\mathcal{P}_0(1 \mp \mathcal{P}_0)}{2}}, \tag{32}$$

where $f_<^{(a)}$ is the focus if $0 < \alpha < \pi/4$ and $f_>^{(a)}$ is the focus if $\pi/4 < \alpha < \pi/2$. The ellipse (26) will have the focus $f^{(b)}$ as being

$$f_{\lessgtr}^{(b)} = \sqrt{\frac{\mathcal{P}_0(1 \pm \mathcal{P}_0)}{2}}, \tag{33}$$

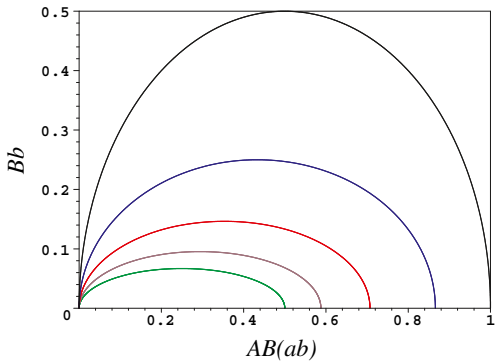

Fig. 4 Graphic of the semiellipse $C_{AB(ab)} \times C_{Bb}$ with $\alpha = \pi/4, \pi/6, \pi/8, \pi/10,$ and $\pi/12$ for the colors *black*, *blue*, *red*, *brown*, and *green*, respectively

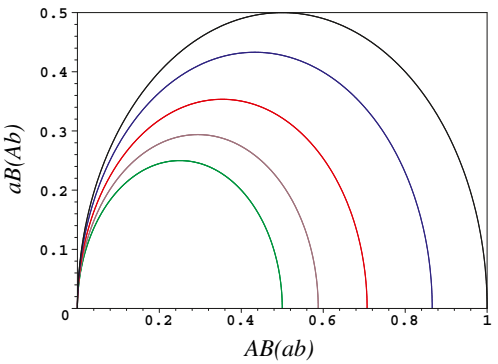

Fig. 6 Graphic of the semicircumference $C_{AB(ab)} \times C_{aB(Ab)}$ with $\alpha = \pi/4, \pi/6, \pi/8, \pi/10$ and $\pi/12$ for the colors *black*, *blue*, *red*, *brown*, and *green*, respectively

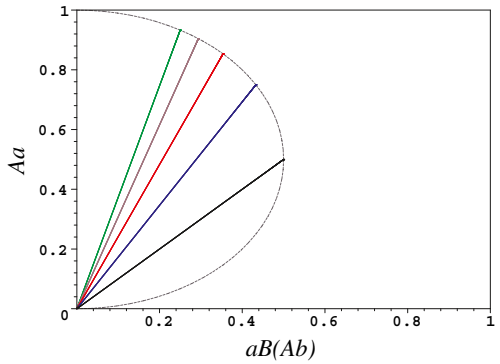

Fig. 7 Graphic of the straight line $C_{aB(Ab)} \times C_{Aa}$ with $\alpha = \pi/4, \pi/6, \pi/8, \pi/10,$ and $\pi/12$ for the colors *black*, *blue*, *red*, *brown*, and *green*, respectively. The *slim violet curve* is the semicircumference $(2C_{Aa} - 1)^2 + (2C_{aB(Ab)})^2 = 1$

where $f_{>}^{(b)}$ is the focus if $0 < \alpha < \pi/4$ and $f_{<}^{(b)}$ is the focus if $\pi/4 < \alpha < \pi/2$, i.e., the opposite case of (32). This happens because the entanglement of the partition Aa (Bb) is generated by the JCM evolution and not by the initial source of entanglement contained in AB. The entanglement generated by the JCM depends on the "quantity" of excitation that will be shared between the respective atom–field. Thus, when $0 < \alpha < \pi/4$, the excitation, in the state represented by (3), will be more likely to be found in the partition Aa. Then, the entanglement generated by the JCM in the partition Aa will be larger than Bb. This is represented in Fig. 5, where C_{Aa} reaches larger values than 0.5 if $0 < \alpha < \pi/4$. In this case, the entanglement in the partition Bb has values below 0.5, as we can observe in Fig. 4. The same analysis is valid in the opposite case, where $\pi/4 < \alpha < \pi/2$. On the other hand, if $\alpha \in (0, \pi/2)$, the eccentricity of the ellipses (25) and (26) are identical, as shown in (31), but the focuses f^a and f^b do not have the same value and do not necessarily lie in the same axis, except for the case $\alpha = \pi/4$ when we have circumferences in both cases. For example, if

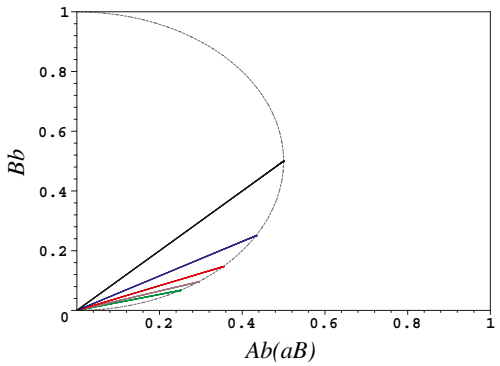

Fig. 8 Graphic of the straight line $C_{Ab(aB)} \times C_{Bb}$ with $\alpha = \pi/4, \pi/6, \pi/8, \pi/10,$ and $\pi/12$ for the colors *black*, *blue*, *red*, *brown*, and *green*, respectively. The *slim violet curve* is the semicircumference $(2C_{Bb} - 1)^2 + (2C_{Ab(aB)})^2 = 1$

$\alpha = \pi/6$, we have $f^b = \sqrt{3}\, f^a$, where f^a (f^b) is over the horizontal (vertical) axis, respectively.

In Section 3.1.3, Eq. (27) represents semicircumferences with radius $C_0/2$. When $\alpha = \pi/4$ ($C_0 = 1$), the limiting curve is obtained. More generally, we can say that a curve defined in its respective diagram $C_{ij} \times C_{kl}$ is always limited by the semicircumference $C_{ij}^2 + C_{kl}^2 = C_0^2$.

The sequential cases, represented by Eqs. (28) and (29), are straight lines with angular coefficient dependent on the initial entanglement. As we did previously, we can write the angular coefficient as functions of the predictability. Equation (28) has angular coefficient $m^{(a)}$ given by

$$m_{\lessgtr}^{(a)} = \left[\frac{1 - \mathcal{P}_0}{1 + \mathcal{P}_0}\right]^{\pm 1/2}, \tag{34}$$

where $m_{<}^{(a)}$ is the coefficient when $0 < \alpha < \pi/4$ and $m_{>}^{(a)}$ is the coefficient if $\pi/4 < \alpha < \pi/2$. Straight lines of Eq. (29) have angular coefficient

$$m_{\lessgtr}^{(b)} = \left[\frac{1 - \mathcal{P}_0}{1 + \mathcal{P}_0}\right]^{\pm 1/2}, \tag{35}$$

where, as in the previous case, $m_{<}^{(b)}$ is the coefficient if $0 < \alpha < \pi/4$ and $m_{>}^{(b)}$ is the coefficient if $\pi/4 < \alpha < \pi/2$. The opposite occurs for (34). This effect is also due to the entanglement given by the JCM as we have already discussed previously in the ellipse Eqs. (25) and (26).

3.2 For the Initial State $|\phi_0\rangle$

Let us now consider the physical system whose initial state is given by Eq. (8). After a time interval t, the state of the system will be (9). In an analogous way as before we determine the concurrences of each pair of qubits. Those are

$$C_{AB} = \max\left[0, C_0 \cos^2(gt) - \gamma_t\right], \tag{36}$$

$$C_{ab} = \max\left[0, C_0 \sin^2(gt) - \gamma_t\right], \tag{37}$$

$$C_{Aa} = \cos^2(\alpha)|\sin(2gt)|, \tag{38}$$

$$C_{Ab} = \max\left[0, \frac{1}{2}C_0|\sin(2gt)| - \gamma_t\right], \tag{39}$$

$$C_{aB} = \max\left[0, \frac{1}{2}C_0|\sin(2gt)| - \gamma_t\right], \tag{40}$$

$$C_{Bb} = \cos^2(\alpha)|\sin(2gt)|, \tag{41}$$

where $\gamma_t = \frac{1}{2}\cos^2(\alpha)\sin^2(2gt)$. Observe that if $0 < \alpha < \pi/4$, we have entanglement sudden death [2–5] or entanglement sudden birth [6].

In this case, we have some interesting situations due to the symmetry of the system. Notice that the partition Aa and Bb will have the same predictability. Thus, the dynamical entanglement supplied by the JCM to Aa or Bb is the

same. Observe that $C_{Aa} = C_{Bb}$. This would not be true if the coupling constant of each JCM were different. Due to that same symmetry, we also have $C_{Ab} = C_{Ba}$. Those relations define straight lines (like the case of Eq. (23)) in their respective diagrams. The other diagrams $C_{ij} \times C_{kl}$, however, are not so simple. That is because the initial state (8) contains the eigenstate $|00\rangle \otimes |00\rangle$ of the Hamiltonian (1), which does not contribute for the entanglement generated by the JCM, i.e., the time evolution of that eigenstate only adds a global phase to it (see Eq. (11)). On the other hand, if the initial state is (2), both the states $|10\rangle \otimes |00\rangle$ and $|01\rangle \otimes |00\rangle$ contribute for the entanglement generated by the JCM in a form of senoidal functions of time in the amplitudes of the state (3) and that is why we obtain conics when we make parametric plots of concurrences.

The next case is in the diagram $C_{ab} \times C_{AB}$. Consider an instant of time when the concurrences C_{AB} and C_{ab} are different from zero at the same time. Then, we can write $C_{AB} = C_0 \cos^2(gt) - \gamma_t$ and $C_{ab} = C_0 \sin^2(gt) - \gamma_t$. Notice that using simple algebra we can write $[C_0 - (C_{AB} + C_{ab})]/\cos^2(\alpha) = \sin^2(2gt)$ and $(C_{AB} - C_{ab})^2/C_0^2 = \cos^2(2gt)$. Summing both, we have

$$\frac{(C_{AB} - C_{ab})^2}{C_0^2} + \frac{C_0 - (C_{AB} + C_{ab})}{\cos^2(\alpha)} = 1. \tag{42}$$

This is a parabola with symmetry axis at 45° of the horizontal axis (C_{ab}). On this axis, the vertex v is localized at point $v_{\lessgtr} = \{0, C_0 - (1 \pm \mathcal{P}_0)/2\}$ and the focus f at $f_{\lessgtr} = \{0, C_0 \mp \mathcal{P}_0\}$, where the index $<(>)$ refers to $0 < \alpha < \pi/4$ $(\pi/4 < \alpha < \pi/2)$, respectively. Because of the entanglement sudden death in the partitions AB and ab whenever $0 < \alpha < \pi/4$, there will only be a segment of the parabola in the diagram $C_{ab} \times C_{AB}$ if the vertex v admits positive values on the axis of the parabola. On the other hand, when the vertex is the origin or admits negative values, we will only have the straight line $C_{AB} = 0$ or $C_{ab} = 0$ (observe Fig. 9 for illustration).

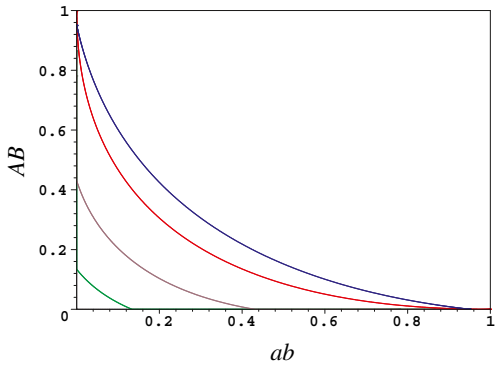

Fig. 9 Graphic of the parabola $C_{ab} \times C_{AB}$ with $\alpha = 3\pi/10, \pi/4, \pi/5,$ and $\pi/6$ for the colors *blue*, *red*, *brown*, and *green*, respectively

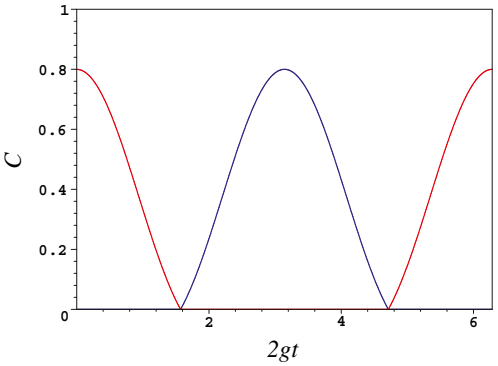

Fig. 10 In $red(blue)$ the graphic of C_{AB} (C_{ab}), respectively, for $\alpha = \arctan(1/2)$

If $\alpha = \arctan(1/2)$, we have $v = \{0, 0\}$ and when the entanglement in one of the partitions disappears, the entanglement of another one resurges, as we see in Fig. 10.

Following the same reasoning, it is clear that if $0 < \alpha < \arctan(1/2)$ (or $\arctan(1/2) < \alpha < \pi/2$) the entanglement in AB disappears before (or after) it appears in ab, respectively (this dynamics is depicted in Fig. 11).

We keep seeking for more relations. Using the sum of Eqs. (36) and (37), squaring them and adding to Eqs. (38) or (41) squared, we get the following ellipse with expression

$$\frac{(C_{AB} - C_{ab})^2}{C_0^2} + \frac{C_{Aa(Bb)}^2}{\cos^4 \alpha} = 1. \tag{43}$$

In Fig. 12, we show that we will always have a segment of the above ellipse, because the entanglement in Aa does not suddenly disappear. If $0 < \alpha < \arctan(1/2)$, the major semiaxis will be parallel to $C_{Aa(Bb)}$. When $\alpha = \arctan(1/2)$, we have a circumference and if

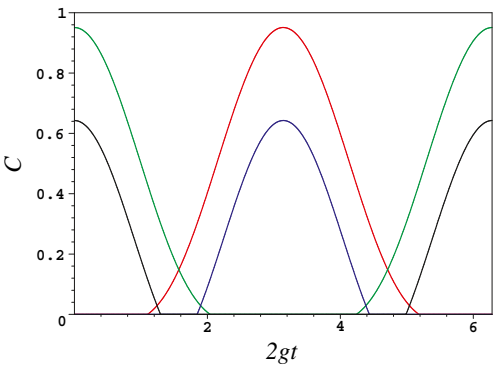

Fig. 11 Graphic of C_{AB} (C_{ab}) in $black(blue)$ when $\alpha = \pi/9 < \arctan(1/2)$, respectively. Graphic of C_{AB} (C_{ab}) in $green(red)$ when $\alpha = \pi/5 > \arctan(1/2)$, respectively

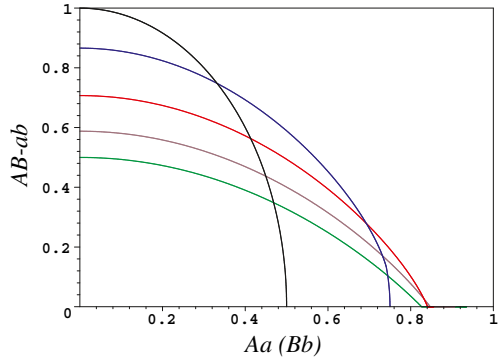

Fig. 12 Graphic of the ellipse $C_{Aa(Bb)} \times (C_{AB} - C_{ab})$ with $\alpha = \pi/4, \pi/6, \pi/8, \pi/10,$ and $\pi/12$ for the colors *black*, *blue*, *red*, *brown*, and *green*, respectively

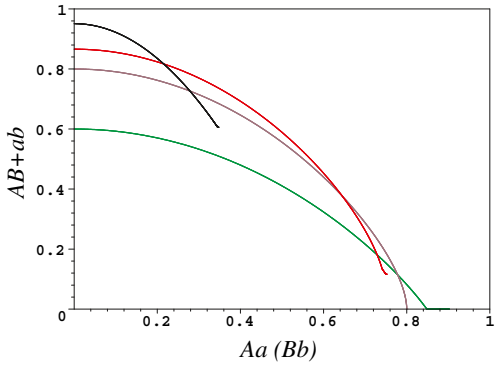

Fig. 13 Graphic of the parabola $C_{Aa(Bb)} \times (C_{AB} + C_{ab})$ with $\alpha = 3\pi/10, \pi/6,$ arctan(1/2), and arctan(1/3) for the colors *black*, *red*, *brown*, and *green*, respectively

arctan$(1/2) < \alpha < \pi/2$, the major semiaxis will be parallel to $C_{AB} - C_{ab}$. The eccentricity of (43) is

$$\bar{\epsilon} = \begin{cases} \sqrt{\dfrac{5\mathcal{P}_0 - 3}{(1+\mathcal{P}_0)}}, & \text{if } 0 < \alpha < \alpha_0 \\ \sqrt{\dfrac{3 - 5\mathcal{P}_0}{4(1-\mathcal{P}_0)}}, & \text{if } \alpha_0 < \alpha < \pi/4 \\ \sqrt{\dfrac{3 + 5\mathcal{P}_0}{4(1+\mathcal{P}_0)}}, & \text{if } \pi/4 < \alpha < \pi/2, \end{cases} \tag{44}$$

where $\alpha_0 = \arctan(1/2)$. The focus is

$$\bar{f} = \begin{cases} \sqrt{(5\mathcal{P}_0 - 3)(1+\mathcal{P}_0)}/2, & \text{if } 0 < \alpha < \alpha_0 \\ \sqrt{(3 - 5\mathcal{P}_0)(1+\mathcal{P}_0)}/2, & \text{if } \alpha_0 < \alpha < \pi/4 \\ \sqrt{(3 + 5\mathcal{P}_0)(1-\mathcal{P}_0)}/2, & \text{if } \pi/4 < \alpha < \pi/2. \end{cases} \tag{45}$$

Observe that when $\alpha = \alpha_0$ we have $\mathcal{P}_0 = 3/5$, $\bar{f} = 0$ and the ellipse becomes a semicircumference. Notice that if $0 < \alpha < \alpha_0$, the entanglement of AB disappears before the appearance of entanglement in ab. However, the entanglement of Aa is given by the JCM and does not remain zero in any finite interval of time. As a result, there will be a time interval such that $C_{AB} - C_{ab}$ will be zero but the entanglement between Aa will not. Thus, C_{Aa} will admit values larger than $C_{AB} - C_{ab}$ and we have the major semiaxis parallel to C_{Aa}.

Consider now the expression used previously, $[C_0 - (C_{AB} + C_{ab})]/\cos^2(\alpha) = \sin^2(2gt)$. Using Eq. (38) or (41), we get another parabola whose equation reads

$$(C_{AB} + C_{ab}) = C_0 - \frac{C_{Aa(Bb)}^2}{\cos^2\alpha}. \tag{46}$$

In Fig. 13, it becomes clear that the vertex $\tilde{v}$ and the focus $\tilde{f}$ are localized on the axis $(C_{AB} + C_{ab})$ at points given by $\tilde{v} = \left\{0, \sqrt{1 - (\mathcal{P}_0)^2}\right\}$ and $\tilde{f}_{\lessgtr} = \left\{0, \sqrt{1 - \mathcal{P}_0} - (1 \pm \mathcal{P}_0)\right\}$. As before, the subindex is $<$ ($>$) if $0 < \alpha < \pi/4$ ($\pi/4 < \alpha < \pi/2$), respectively. We always have a segment of this parabola in the diagram $(C_{AB} + C_{ab}) \times C_{Aa(Bb)}$, because its vertex is limited between 0 and 1. We also know that $(C_{AB} + C_{ab})$ will not be zero if $\alpha_0 < \alpha < \pi/2$ and in this interval the parabola does not touch the axis $C_{Aa(Bb)}$.

And last but not least, we can write $|\sin(2gt)| = C_{Aa(Bb)} \cos^2\alpha$ from Eqs. (38) or (41) and substitute in (39) or (40). With some simplifications, we have

$$C_{Ab(aB)} + \frac{1}{2\cos^2\alpha}\left(C_{Aa(Bb)} - \frac{C_0}{2}\right)^2 = \frac{C_0^2}{8\cos^2\alpha}. \tag{47}$$

This equality, like the previous case, represents a parabola with vertex $\breve{v}$ and focus $\breve{f}$ localized at the points

$$\breve{v}_{\lessgtr} = \left\{\frac{\sqrt{1-\mathcal{P}_0^2}}{2}, \frac{(1 \mp \mathcal{P}_0)}{2}\right\},$$

$$\breve{f}_{\lessgtr} = \left\{\frac{\sqrt{1-\mathcal{P}_0^2}}{2}, \frac{\mp\mathcal{P}_0}{2}\right\}.$$

The subindex follows the previous notation. The parabola of Eq. (47) touches twice the axis $C_{Aa(Bb)}$ when $0 < \alpha \leq \alpha_0$. This happens because if $0 < \alpha < \alpha_0$, there is entanglement sudden death in the partition $C_{Ab(aB)}$. If $\alpha_0 < \alpha < \pi/2$, on the other hand, there is not sudden death and the segment of the parabola only touches the axis $C_{Aa(Bb)}$ at the origin, as shown in Fig. 14.

4 The Entanglement Surface

In the previous section, we have explored the diagram $C_{ij} \times C_{kl}$ for two different initial states. Because of the unitary evolution of the physical model and the existence of an entanglement invariant [16], it is relevant to analyze the three-dimensional diagram $C_{ij} \times C_{ik} \times C_{il}$ for the ith qubit.

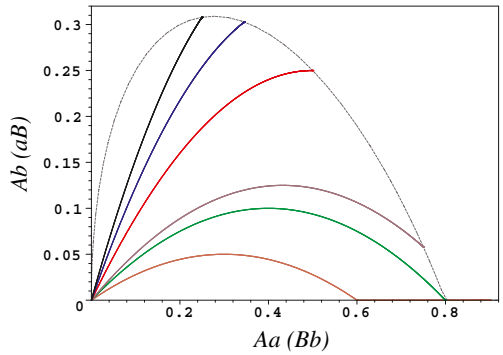

Fig. 14 Graphic of the parabola $C_{Aa(Bb)} \times C_{Ab(aB)}$ with $\alpha = \pi/3, 3\pi/10, \pi/4, \pi/6, \arctan(1/2)$, and $\arctan(1/3)$ for the colors *black*, *red*, *brown*, *green*, and *orange* respectively

First, we analyze such diagram for the atom A. For the initial state (2), the concurrences between the atom A and any other qubit are given by Eqs. (16), (18), and (19). If we make the parametric graphics of this concurrences, we have curves, for a determined value of α, in a diagram $C_{AB} \times C_{Aa} \times C_{Ab}$, as showed in Fig. 15. Naturally, if we look at the projections of this curves in the planes $C_{AB} \times C_{Aa}$, $C_{AB} \times C_{Ab}$ and $C_{Aa} \times C_{Ab}$, we get the graphics drawn in Figs. 5, 6, and 7, respectively. If we draw all the possible curves (varying α from 0 to $\pi/2$) in the diagram $C_{AB} \times C_{Aa} \times C_{Ab}$, we have a surface in that space depicted in Fig. 16. A point over that surface informs how much entanglement there is in each one of the partitions AB, Aa, and Ab. If now we consider the initial state (8) and draw the parametric graphics, for a few values of α, in a diagram $C_{AB} \times C_{Aa} \times C_{Ab}$, we also have curves in that diagram, as depicted in Fig. 17.

As in the previous case, we can draw all possible curves in the diagram $C_{AB} \times C_{Aa} \times C_{Ab}$ if we vary α from 0 to $\pi/2$ and we find an entanglement surface, see Fig. 18. Points

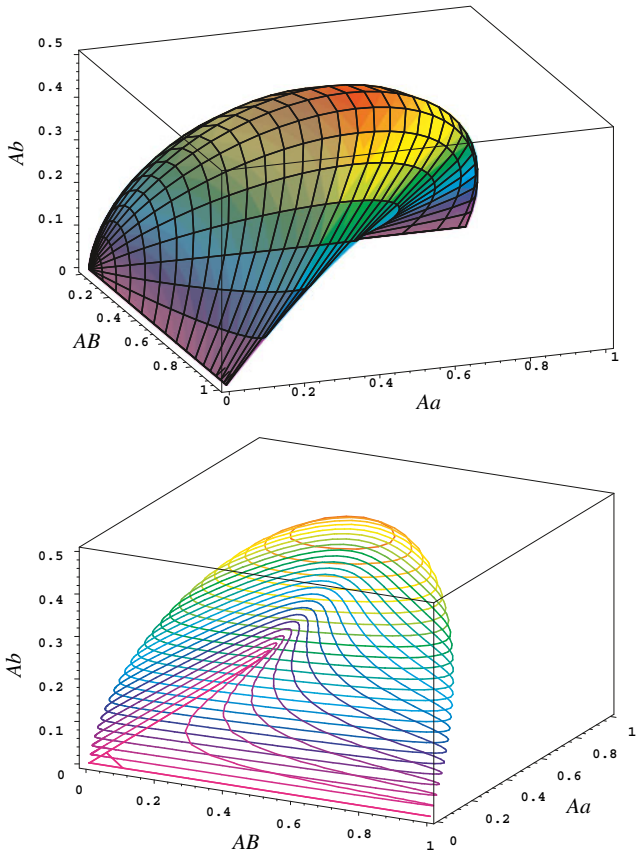

Fig. 16 Entanglement surface for the atom A in the diagram $C_{AB} \times C_{Aa} \times C_{Ab}$ for the initial state (2)

over this surface also gives how much entanglement there is in each of the subsystems AB, Aa, and Ab.

This same conclusions are also true for B, a, and b. So, in a general way, we can say that any trajectory in the diagrams

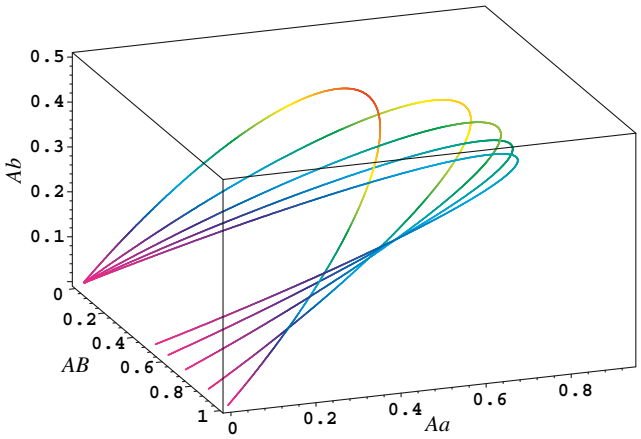

Fig. 15 Graphic of the diagram $C_{AB} \times C_{Aa} \times C_{Ab}$ for the atom A and initial state (2). From the superior curve to the inferior, we have, respectively, $\alpha = \pi/4, \pi/6, \pi/8, \pi/10$, and $\pi/12$

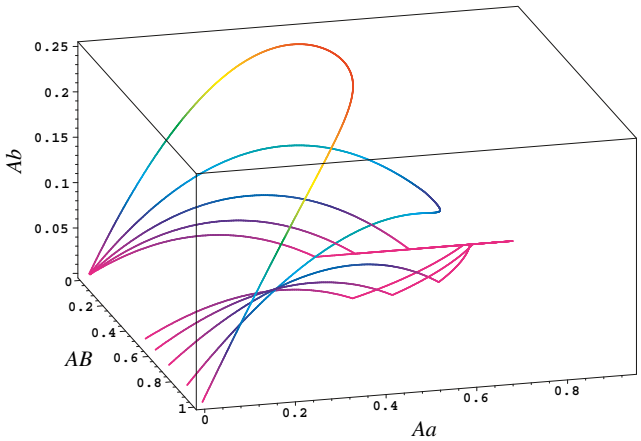

Fig. 17 Graphic of the diagram $C_{AB} \times C_{Aa} \times C_{Ab}$ for the initial state (8), with $\alpha = \pi/4, \pi/6, \pi/8, \pi/10$, and $\pi/12$

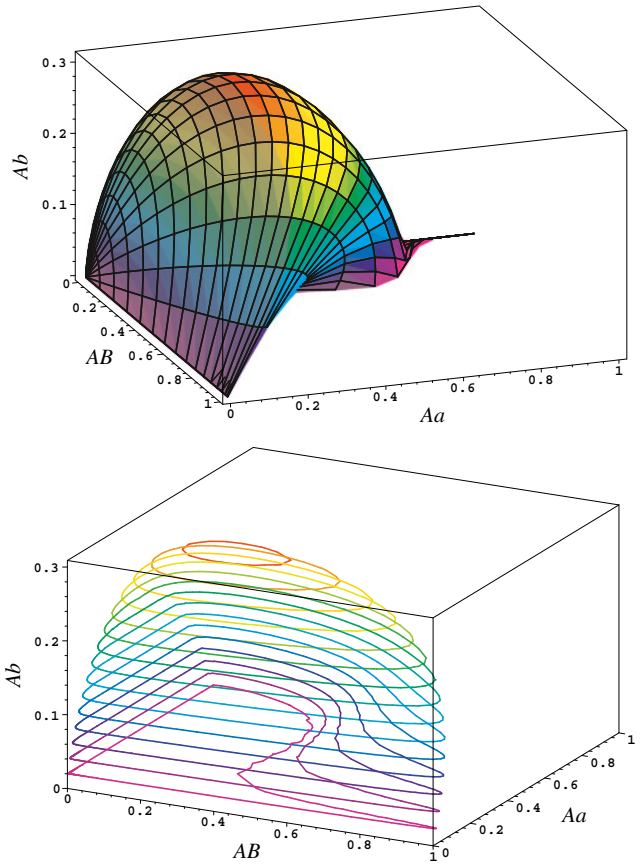

Fig. 18 Entanglement surface of the atom A in the diagram $C_{AB} \times C_{Aa} \times C_{Ab}$ for the initial state (8)

$C_{ij} \times C_{ik}$, $C_{ij} \times C_{il}$ and $C_{ik} \times C_{il}$ belongs to the surface in $C_{ij} \times C_{ik} \times C_{il}$ and they are projections in its respective diagrams, where i, j, k, and l are the four qubits (A, B, a, and b) of the system.

5 Hypersphere Shell of the Entanglement Dynamics

Next, we are going to use a result already obtained in [8] and [19]. In these references, they observed that for the initial state (2), we have $C_{AB}^2 + C_{Ab}^2 + C_{aB}^2 + C_{ab}^2 = C_0^2$. Without loss of generality, we can sum in both sides the term $C_{Aa}^2 + C_{Bb}^2$ and this yields $C_{AB}^2 + C_{Ab}^2 + C_{aB}^2 + C_{ab}^2 + C_{Aa}^2 + C_{Bb}^2 = C_0^2 + \left(\cos^4\alpha + \sin^4\alpha\right)\sin^2(2gt)$. This last expression can be transformed in the inequality $C_{AB}^2 + C_{Ab}^2 + C_{aB}^2 + C_{ab}^2 + C_{Aa}^2 + C_{Bb}^2 \leq C_0^2 + \left(\cos^4\alpha + \sin^4\alpha\right)$. Now, if we use simple trigonometric relations and the predictability, we can rewrite this equation as

$$C_{AB}^2 + C_{Ab}^2 + C_{aB}^2 + C_{ab}^2 + C_{Aa}^2 + C_{Bb}^2 \leq 1 + \frac{C_0^2}{2}, \quad (48)$$

which is a hypersphere with radius $\sqrt{\left(2 + C_0^2\right)/2}$ in a space where the axes are the concurrences between pairs of qubits. Besides, we can generalize the above inequality to

$$C_0^2 \leq C_{AB}^2 + C_{Ab}^2 + C_{aB}^2 + C_{ab}^2 + C_{Aa}^2 + C_{Bb}^2 \leq 1 + \frac{C_0^2}{2}, \quad (49)$$

which defines a limited region (a hypersphere shell) inside the hypersphere defined by Eq. (48). Thus, any curve in a diagram where the axes are concurrences between pairs of qubits and the initial state is (2) will lie either on the surface or in the interior of the hypersphere shell (49). So, we can speculate that, in the same way that curves in diagrams $C_{ij} \times C_{ik}$ are projections of curves of $C_{ij} \times C_{ik} \times C_{il}$, the surface defined in $C_{ij} \times C_{ik} \times C_{il}$ is a projection of the surface of a hypersphere that is in a space of greater dimension.

We can make the same analysis for the initial state (8). However, in that case [8, 19], we have only the inequality $0 \leq C_{AB}^2 + C_{Ab}^2 + C_{aB}^2 + C_{ab}^2 \leq C_0^2$ and, as done previously, we can sum both sides with the term $C_{Aa}^2 + C_{Bb}^2 = [1 + \cos(2\alpha)]^2 \sin^2(2gt)/2$. With a simple algebra, we can express the result of this sum in the inequality $0 \leq C_{AB}^2 + C_{Ab}^2 + C_{aB}^2 + C_{ab}^2 + C_{Aa}^2 + C_{Bb}^2 \leq C_0^2 + [1 + \cos(2\alpha)]^2/2$. We have the predictability $\mathcal{P}_0$ equals to $\cos(2\alpha)$ if $0 < \alpha < \pi/4$ and $-\cos(2\alpha)$ if $\pi/4 \leq \alpha \leq \pi/2$. Using this and $C_0^2 + \mathcal{P}_0^2 = 1$, we can rewrite the inequality as

$$0 \leq C_{AB}^2 + C_{Ab}^2 + C_{aB}^2 + C_{ab}^2 + C_{Aa}^2 + C_{Bb}^2 \leq 1 + \frac{C_0^2}{2} \pm \mathcal{P}_0, \quad (50)$$

where on the right-hand side of the equation, we will have $\left(1 + C_0^2/2 + \mathcal{P}_0\right)$ when $0 < \alpha < \pi/4$ and $\left(1 + C_0^2/2 - \mathcal{P}_0\right)$ when $\pi/4 \leq \alpha \leq \pi/2$. This inequality must be valid during the whole evolution and, in a space defined by the axes corresponding to the concurrences C_{ij}. We have the radius of the hypersphere given by

$$R_{\gtrless} = \sqrt{1 + \frac{C_0^2}{2} \pm \mathcal{P}_0}, \quad (51)$$

where we have $R_>$ ($R_<$) when $0 < \alpha < \pi/4$ ($\pi/4 \leq \alpha \leq \pi/2$), respectively. It is noteworthy that for $0 < \alpha < \pi/4$, there is sudden death of entanglement in few partitions. On the other hand, for $\pi/4 \leq \alpha \leq \pi/2$, there is not sudden death for any partition. Thus, we have $R_>$ when there is sudden death and $R_<$ otherwise. Note that for $0 < \alpha < \arctan(1/2)$ there will be a time interval $\Delta\tau = \left[\arccos\left(\sqrt{\tan\alpha}\right) - \arcsin\left(\sqrt{\tan\alpha}\right)\right]/g$ where $C_{AB} = C_{ab} = C_{Ab} = C_{aB} = 0$ (as observed in [6]). Since the hypersphere is defined by the concurrences between pairs of qubits, one would intuitively expect, in this conditions and during the time interval $\Delta\tau$, to obtain $R_<$ in place of $R_>$ since only C_{Aa} and C_{Bb} are different from zero. The increasing of the average radius is a consequence of

the dynamical entanglement C_{Aa} and C_{Bb}. When $0 < \alpha < \pi/4$, the entanglement of the partitions Aa and Bb will attain maximum values between 1/2 and 1. Thus, the maximum value of $C_{Aa}^2 + C_{Bb}^2$ will be between 1/2 and 2, contributing substantially to the inequality (50).

6 The Effect of Perturbation on Conics

In this section, we consider the effect of decoherence in order to see how some conics of Section 3 are affected. We consider the two cavities decaying freely, i.e., they both interact with a reservoir at zero temperature. This is a model closer to experimental reality.

The solution of the master equation for the initial state (2) gives us the density matrix for this case. We take the partial trace over the subsystems in order to obtain the following concurrences

$$C_{AB} = e^{-rz}|\sin 2\alpha|\left[\cos\left(\frac{z}{2}\right) + r\sin\left(\frac{z}{2}\right)\right]^2, \quad (52)$$

$$C_{Aa} = e^{-rz}\sqrt{1+r^2}\cos^2\alpha|r(1-\cos z) + \sin z|, \quad (53)$$

$$C_{Bb} = e^{-rz}\sqrt{1+r^2}\sin^2\alpha|r(1-\cos z) + \sin z|, \quad (54)$$

$$C_{Ab} = \frac{1}{2}e^{-rz}\sqrt{1+r^2}|\sin 2\alpha||r(1-\cos z) + \sin z|, \quad (55)$$

$$C_{aB} = \frac{1}{2}e^{-rz}\sqrt{1+r^2}|\sin 2\alpha||r(1-\cos z) + \sin z|, \quad (56)$$

$$C_{ab} = e^{-rz}(1+r^2)|\sin 2\alpha|\sin^2\left(\frac{z}{2}\right), \quad (57)$$

where k is the decay constant, $\Omega = \sqrt{4g^2 - k^2}$ is the Rabi frequency, $r = \frac{k}{\Omega}$ is the ratio between them, and $z = \Omega t$. We recover Eqs. (16)–(21) in the limit $k \to 0$.

Surprisingly enough, the curves (23), (24), (28), and (29) are not affected by this type of external coupling considered. On the other hand, if we consider one of the ellipses of Section 3.1.1, we see that its size decreases with time. This result shows what we would expect, i.e., the decoherence destroys the entanglement between the atoms and the entanglement between an atom and its cavity (see Fig. 19a). Of course, this effect also depends on how large r is. Figure 19a, b shows examples where we see that the semiaxes go to zero in less time with the increasing of the external coupling.

The straight line of Eq. (22) is also affected by the environment as we can see in Fig. 20. In this case, the intersection of the lines with the axes C_{AB} and C_{ab} shows that the initial available entanglement (C_0) is decreasing because the environment is monitoring the system.

Furthermore, we can notice by observing Figs. 19a, b and 20 that the eccentricity of the ellipse and the angular

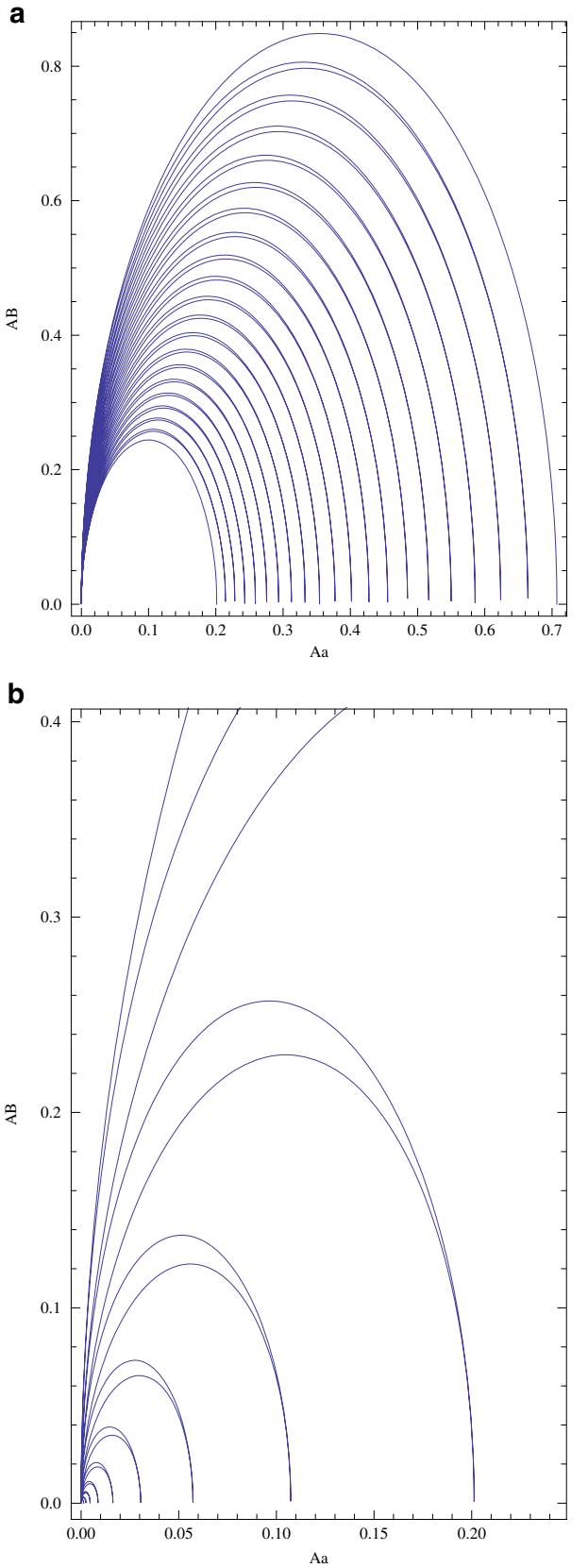

Fig. 19 **a** Graphic of the semiellipse $C_{AB} \times C_{Aa}$ with $\alpha = \pi/8$, $r = 0.01$ and $z \in [0, 40\pi]$. **b** Graphic of the semiellipse $C_{AB} \times C_{Aa}$ with $\alpha = \pi/8$, $r = 0.1$, and $z \in [0, 20\pi]$

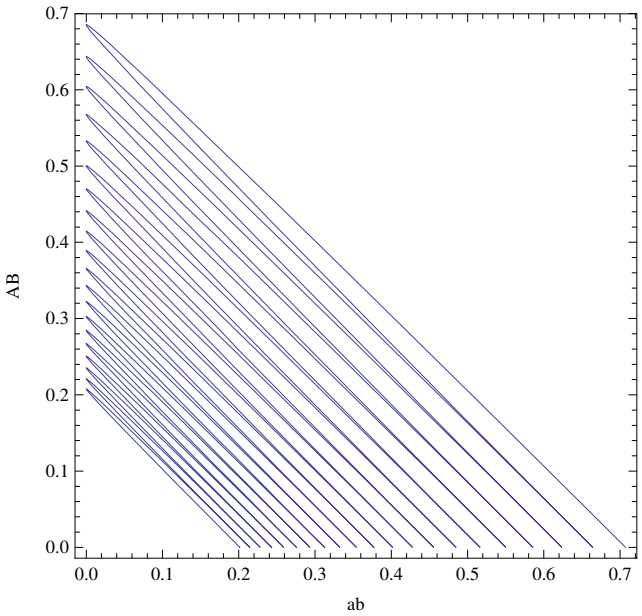

Fig. 20 Graphic of the straight line $C_{AB} \times C_{ab}$ with $\alpha = \pi/8$, $r = 0.01$, and $z \in [0, 40\pi]$

coefficient do not change considerably with time. Therefore, it is possible to relate those with predictability as done in Section 3.

7 Conclusions

We have presented a detailed study of the geometric character of the entanglement dynamics of two pairs of qubits evolving according to the DJCM. Although this is an analytically solvable simple model, it exhibits a very rich dynamical structure which we explored here in order to give a geometric meaning to the entanglement dynamics. As it became clear, its very difficult to generalize our results to other more sophisticated models or initial conditions. However, we strongly believe that there is an intimate connection between the average radius of the hypersphere and the phenomenon of sudden death of entanglement. We hope to have provided for a tool which might aid experimentalists given that DJCM is within today's available technology.

References

1. A. Einstein, E. Podolsky, N. Rosen, Phys. Rev. **47**, 777 (1935)
2. T. Yu, J. Eberly, Phys. Rev. Lett. **93**, 140404 (2004)
3. M. Santos, P. Milman, L. Davidovich, N. Zagury, Phys. Rev. A **73**, 040305 (2006)
4. T. Yu, Phys. Lett. A **361**, 287 (2007)
5. Y.J. Zhang, Z.X. Man, Y.J. Xia, J. Phys. B At. Mol. Opt. Phys. **42**, 095503 (2009)
6. C. Lópes, G. Romero, F. Lastra, E. Solano, J. Retamal, Phys. Rev. Lett. **101**, 080503 (2008)
7. J.S. Zhang, J.B. Xu, Opt. Commun. **282**, 3652 (2009)
8. S. Chan, M. Reid, Z. Ficek, J. Phys. B At. Mol. Opt. Phys. **43**, 215505 (2010)
9. E. Jaynes, F. Cummings, Proc. IEEE **51**, 89 (1963)
10. M. Tavis, F. Cummings, Phys. Rev. **170**, 379 (1968)
11. M. Yönaç, T. Yu, J. Eberly, J. Phys. B At. Mol. Phys. **39**, S621 (2006)
12. H.T. Cui, K. Li, X.X. Yi, Phys. Lett. A **365**, 44 (2007)
13. Z.X. Man, Y.J. Xia, N. An, J. Phys. B At. Mol. Phys. **41**, 085503 (2008)
14. D. McHugh, M. Ziman, V. Bužek, Phys. Rev. A **74**, 042303 (2006)
15. D. Cavalcanti, J.G. Oliveira Jr., J.G. Peixoto de Faria, M. Terra Cunha, M. França Santos, Phys. Rev. A **74**, 042328 (2006)
16. I. Sainz, G. Björk, Phys. Rev. A **76**, 042313 (2007)
17. M. Yönaç, T. Yu, J. Heberly, J. Phys. B At. Mol. Phys. **40**, S45 (2007)
18. J.L. Guo, H.S. Song, J. Phys. A Math. Theor. **41**, 085302 (2008)
19. S. Chan, M. Reid, Z. Ficek, J. Phys. B Atomic Mol. Phys. **42**, 065507 (2009)
20. Z.X. Man, Y.J. Xia, N.B. An, Eur. Phys. J. D **53**, 229 (2009)
21. W.K. Wootters, Phys. Rev. Lett. **80**, 2245 (1998)
22. M. Jakob, J. Bergou. Opt. Commun. **179**, 337 (2000)